Pergamon

Int. J. Heat Mass Transfer. Vol. 39, No. 16, pp. 3333–3346, 1996

0017–9310/96 $15.00 + 0.00

PII: S0017–9310(96)00030–0

Turbulent velocity field in isothermal and heated liquid flow through a vertical annular channel

V. VELIDANDLA, S. PUTTA and R. P. ROY†

Arizona State University, Department of Mechanical and Aerospace Engineering, Tempe, AZ 85287-6106, U.S.A.

(*Received* 3 *October* 1995 *and in final form* 27 *December* 1995)

Abstract—Time-mean axial and radial velocities, axial and radial turbulent intensities and the single-point cross-correlation between axial and radial turbulent velocity fluctuations (~axial Reynolds shear stress) were measured in unheated and heated turbulent upflow of liquid Refrigerant-113 through a vertical concentric annular channel. Time-mean temperature and temperature fluctuation intensity were measured in the heated flows. A two-component laser Doppler velocimeter was used for the velocity measurements and microthermocouples for temperature measurement. Results are reported for Reynolds numbers of 18 000, 28 450 and 40 480 at inner wall heat fluxes of 0, 9000 and 16 000 W m^{-2}. Buoyancy effects were found on the time-mean velocity and turbulence fields, even at very low values of Gr/Re^2. Mechanisms suggested by Petukhov and Polyakov explain these effects. The results should be useful in the development and validation of turbulence models for such flows. Copyright © 1996 Elsevier Science Ltd.

INTRODUCTION

Turbulent liquid flow and heat transfer in heated annular channels are of interest because of their many applications in engineering systems—for example, heat exchangers, nuclear reactor cores, etc. One seeks to understand the characteristics of turbulence in such flow, develop a model of the flow field, and utilize the model in the design of equipment. In an earlier effort, we had performed measurements, by constant temperature hot-film anemometry (CTA), of the velocity and temperature fields in turbulent upflow of liquid through a vertical annular channel whose inner wall was heated, Hasan *et al.* [1]. However, these measurements appear to have suffered from several shortcomings: (i) the probe was rather large compared to the annulus spacing, precluding measurement near the walls and quite possibly disturbing the flow field, and (ii) compensation of the effect of temperature fluctuations on the measured velocity was inadequate in some cases resulting in inaccuracy. The CTA system was subsequently replaced by a laser Doppler velocimeter (LDV) system with the intent of rectifying the shortcomings.

Measurements of the velocity field in isothermal turbulent flow of air through annuli have been reported by Brighton and Jones [2], Quarmby [3], Lawn and Elliott [4], Rehme [5], and Wilson [6]. Heikal *et al.* [7] measured the velocity field in heated flow of air through an annular channel. Computations of the turbulent velocity field in heated annuli were performed by Wilson and Medwell [8], Hanjalic [9], and Malik and Pletcher [10].

In the present study, LDV measurements were carried out initially in the upward flow of isothermal liquid through a vertical concentric annular channel at three Reynolds numbers. Measurements could be made much closer to the inner wall of the annulus compared with our earlier CTA work. Radial distributions of the time-mean axial velocity $\overline{U}$, time-mean radial velocity $\overline{V}$, axial turbulent intensity u', radial turbulent intensity v', and the single-point cross-correlation $\overline{uv}$ (~axial Reynolds shear stress) were measured at an axial location in the channel where the flow was hydrodynamically fully developed. These isothermal measurements served as the base for the subsequent heated flow measurements.

The heated flow experiments were conducted at the same three Reynolds numbers. First, the liquid temperature field (mean and fluctuation intensity) was measured at the same channel axial location in each experiment. In addition to characterizing the turbulent temperature field, these measurements were necessary for conducting LDV measurement in heated liquid flow.

Our main objective was to obtain results that would be useful in the development and validation of models for the heated turbulent flow of a moderate Prandtl number (≈5–10) liquid. Since, depending upon the Reynolds number and Grashof number, the effects of buoyancy on the velocity field can be significant [11, 12] it was deemed important to quantify these effects at low values of Gr/Re^2 (<0.1) and then to explain them.

† Author to whom correspondence should be addressed.

NOMENCLATURE

D_h annulus hydraulic diameter, $2(r_o - r_i)$
e turbulent energy
E nondimensional turbulent energy, $e/\bar{U}_{bulk}^2$
g gravitational acceleration
G mass velocity
Gr Grashof number, $g\beta_f(\bar{T}_{wi} - \bar{T}_{bulk})\bar{D}_h^3/\nu_f^2$
k_f liquid thermal conductivity
L^* nondimensional turbulence length scale
p, p_o pressure, reference pressure
P^* nondimensional pressure, $(p - p_0)/\rho_f \bar{U}_{bulk}^2$
Pr Prandtl number
q''_{wi} heat flux at annulus inner wall
$r; r^*$ radial coordinate; nondimensional radial coordinate, $(r - r_i)/D_h$
R^* nondimensional radial coordinate, $(r - r_i)/(r_o - r_i)$
Re Reynolds number, $\bar{U}_{bulk} D_h/\nu_f$, based on liquid properties at $\bar{T}_{in}$
$\bar{T}, t$ time-mean liquid temperature, temperature fluctuation
$\bar{T}^*$ nondimensional mean liquid temperature, $(\bar{T} - \bar{T}_{in})k_f/q''_{wi}D_h$
$\bar{T}_{bulk}$ mixed-mean liquid temperature
$\bar{T}_{wi}$ time-mean temperature of inner wall
t^* nondimensional liquid temperature fluctuation, $t/(\bar{T}_{wi} - \bar{T}_{bulk})$
t' temperature fluctuation intensity
$\bar{U}, \bar{V}$ time-mean axial velocity, time-mean radial velocity
u, v axial velocity fluctuation, radial velocity fluctuation
u', v' axial turbulent intensity, radial turbulent intensity
$\bar{U}_{bulk}$ mixed-mean axial velocity
u^+ nondimensional time-mean axial velocity in wall coordinate, $\bar{U}/u_{\tau_i}$
u_{τ_i} friction velocity at annulus inner wall
$\bar{U}^*; \bar{V}^*$ nondimensional time-mean axial velocity, $\bar{U}/\bar{U}_{bulk}$; nondimensional time-mean radial velocity $\bar{V}/\bar{U}_{bulk}$
$u^*; v^*$ nondimensional axial velocity fluctuation, $u/\bar{U}_{bulk}$; nondimensional radial velocity fluctuation, $v/\bar{U}_{bulk}$
y normal distance from inner wall
y^+ nondimensional normal distance in wall coordinate from inner wall, yu_{τ_i}/ν_f
$z; z^*$ axial coordinate; nondimensional axial coordinate, z/D_h.

Greek symbols

α radius ratio of annulus, r_i/r_o
β nondimensional location of zero axial Reynolds shear stress, $r(\tau = 0)/r_o$
β_f volumetric coefficient of thermal expansion for liquid
ν_f liquid kinematic viscosity
ρ_f liquid density
τ, τ_{wi} axial Reynolds shear stress, shear stress at inner wall
ε eddy kinematic viscosity
Θ nondimesional time-mean liquid temperature, $(\bar{T} - \bar{T}_{in})/(\bar{T}_{wi} - \bar{T}_{bulk})$.

Subscripts

bs backscatter
i, o annulus inner wall, outer wall
in channel inlet
rr retro-reflect
z axial component.

THE EXPERIMENTS

The experimental rig has been described elsewhere [13]. Refrigerant-113 (R-113) was the working liquid. Its volumetric flow rate through the annular test section was measured by a turbine flow meter (EGG Flow Technology). Also monitored during the experiments were the liquid temperatures at test section inlet and exit (by copper–constantan thermocouples) and the inlet and exit pressures (by Bourdon-tube pressure gauges).

The test section

Figure 1 shows, schematically, the *measurement section* of the 3.66 m long concentric annular channel. The inner tube of the entire channel was of 304 stainless steel (i.d. = 14.60 mm, o.d. = 15.80 mm). The 0.521 m long outer tube of the measurement section was of optical quality quartz (i.d = 37.86 mm, o.d. = 41.80 mm). The outer tube of the remainder of the channel was of transparent pyrex glass (i.d. = 38.1 mm, o.d. = 47.0 mm). The measurement plane (m.p.) was 0.424 m ($\approx$19 hydraulic diameters) downstream of the measurement section entrance†, this entrance being in turn 1.51 m downstream of the start of the 2.75 m heated length of the channel. The inner tube could be heated over this 2.75 m length by direct current. A 0.91 m unheated length was provided upstream of the heated length.

† The effect of the slight mismatch ($\approx$0.2 mm) between the inner diameters of the quartz tube and the upstream pyrex tube on the liquid velocity field at the m.p. may thus be assumed to be negligible.

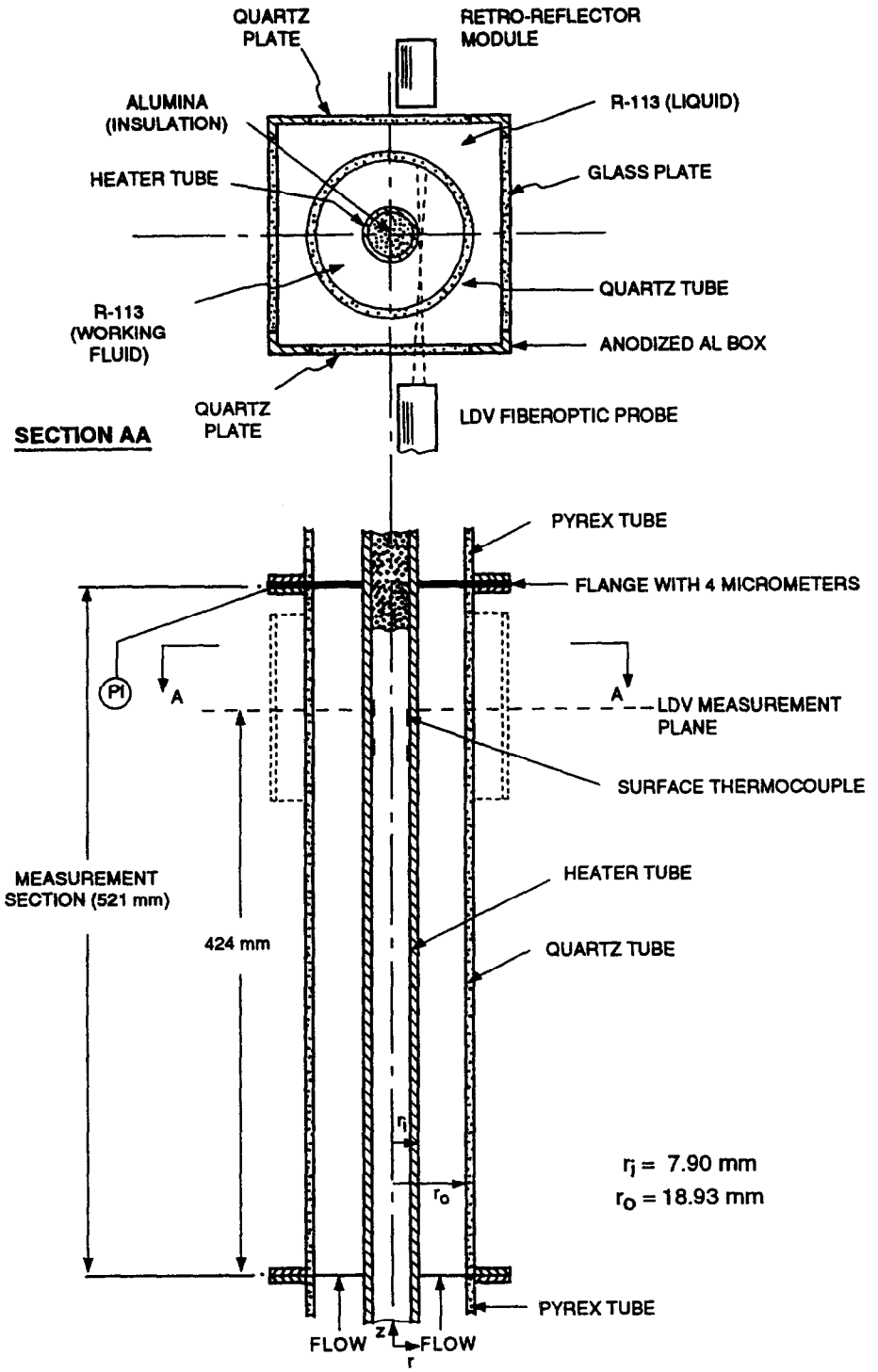

Fig. 1. The annular test section.

Concentricity of the channel was maintained by means of four cruciform vane assemblies, each assembly consisting of four 9 mm long and 1 mm thick stainless steel vanes welded to the inner tube. The nearest vane assembly upstream of the m.p. was about 31 hydraulic diameters away. Concentricity of the measurement section was further ensured by means of a flange equipped with four stainless steel vanes, each traversable by a micrometer, located immediately downstream of the section.

Liquid pressure at the m.p. was measured by a test gauge (Omega, 0–1200 kPa range, 1.4 kPa resolution).

Four copper–constantan surface thermocouples (RdF Corporation) were installed on the inner wall of the heater tube which was then filled with aluminum oxide powder insulation.

An anodized aluminum box with flat front and side quartz windows served as a jacket around a 15 cm length of the measurement section (Fig. 1). This box was filled with liquid R-113 to alleviate laser beam refraction at the outer wall of the quartz tube.

The entire test section except for the length enclosed by the aluminum box was insulated with 50 mm thick jacketed fiberglass wool.

Microthermocouples

The chromel–alumel microthermocouples used to measure the liquid temperature distribution (mean, fluctuation intensity) in the annular channel and in the aluminum box (mean only) have been described by Beckman *et al.* [14]. The time constant of each of these microthermocouples in conjunction with the associated amplifier/filter is less than 3 ms.

The mean temperature distribution in the liquid is vital to the tracing of the LDV beam paths. The liquid temperature fluctuation intensity is an important feature of the turbulence. It also enables estimation of the magnitude of the liquid refractive index fluctuation.

The two-component LDV system

The LDV system (TSI) consisted of a 100 mW Argon-Ion laser and an 83 mm fiberoptic probe (250 mm focal length) equipped with a backscatter light detector. The system also contained a retro-reflector module consisting of a reflecting prism and a focusing lens. This module could be used to direct the forward-scattered light from the LDV measuring volume back to the backscatter detector†. The probe and the retro-reflector module were mounted on independent three-dimensional traverse mechanisms, each mechanism also containing a rotational stage. White nylon particles of 3–7 μm size were used to seed the flow.

There is a significant mismatch between the refractive indices of liquid R-113 and quartz. For example, at 31.2°C the refractive index of liquid R-113 is 1.351 and that of quartz 1.458, with the former index depending on temperature. At the inner and outer walls of the quartz tube, therefore, refractive index mismatches existed in both isothermal and heated flow experiments. Furthermore, in the heated flow experiments, the liquid mean refractive index varied spatially in the annulus. There was also some (albeit much less) mean refractive index variation in the aluminum box liquid. To account for these and locate the LDV measuring volume (m.v.) at desired positions in the annulus, a beam tracing algorithm and a beam steering module were used, Velidandla *et al.* [15].

In isothermal flow of liquid R-113, the LDV probe volume was calculated to be an ellipsoid with minor axes about 0.1 mm long (in the r–z plane) and major axis (perpendicular to the r–z plane) about 0.9 mm long. The actual measuring volume is more difficult to determine and was assumed to coincide with the probe volume. In the arrangement shown in Fig. 1, the minor axes defined the radial and axial positions of measurement in the test section.

One other refractive index-related issue required attention. It involves the cumulative (along the beam path) effect of the random fluctuations in the liquid refractive index, caused by turbulent temperature fluctuations, on the crossing of the beams and random movement of the fringes in the m.v. Short beam paths (for example, less than three times the integral length scale‡) and the use of frequency shifter and Bragg cell have been recommended as potential remedies for this problem [16].

It was important to consider whether significant statistical bias could be present in the velocity data. *Data density* defined as (data validation rate) · (Taylor time microscale) is an important parameter in this regard [17]. In our experiments, the data density was found to be in the *intermediate range* (between 0.05 and 1) throughout the flow field, except very near the inner wall where it often was lower than 0.05 (especially in the heated flow experiments due to thermophoresis of seed particles [18]). The recommended method for removal of velocity bias at intermediate data densities is residence time weighting. Residence time weighting could not be done in our signal processor. As such, it became necessary to determine the extent of velocity bias in the measurements. This was done by using the signal processor as a *controlled processor* in selected experiments.

Calibration of the LDV system. Some of the initial LDV data were compared with data obtained in an almost identical measurement section by constant temperature anemometry (CTA) [1]. A miniature three-sensor hot-film probe had been used for CTA measurements.

Firstly, radial distributions of liquid time-mean axial and radial velocities, axial and radial turbulent intensities, and $\overline{uv}$ at the m.p. were compared for several isothermal experiments. As mentioned earlier, it was possible to measure much closer to the inner wall by LDV. In the region common to LDV and CTA measurements, good agreement was found except for some distortion that appeared in the CTA turbulent intensity data near the walls. Disturbance caused by the CTA probe may have been the reason for this.

Secondly, comparison was made for several heated flows. Figure 2(a, b) contains the radial distribution of liquid mean axial velocity and axial turbulent inten-

† The data rate in this mode was usually substantially higher than that in the backscatter light collection mode.

‡ This criterion, of course, may not be possible to satisfy in many experiments.

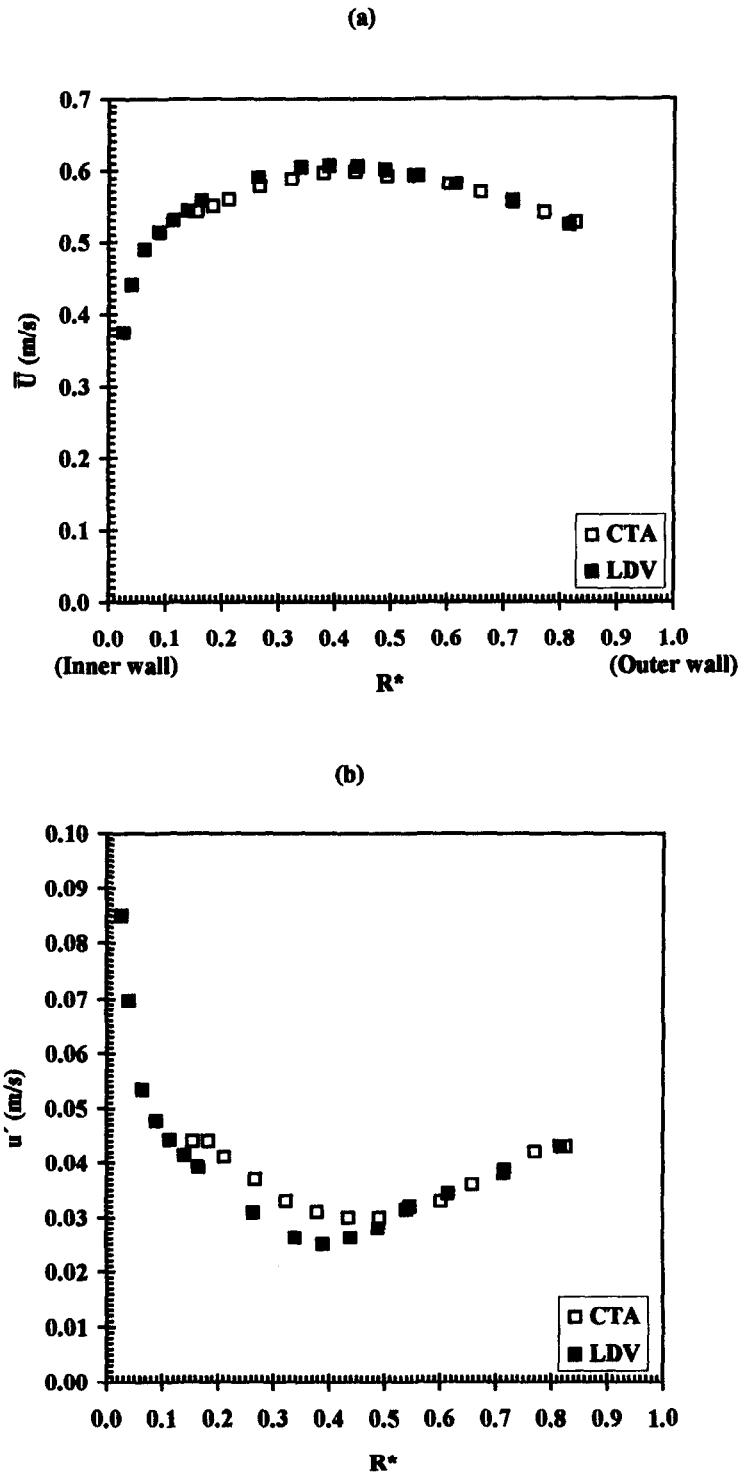

Fig. 2. Measurements in heated flow by LDV and CTA, (a) mean axial velocity, (b) axial turbulent intensity.

sity at the m.p. for the following two flows:

	LDV expt.	CTA expt.
mass velocity	826 kg m^{-2} s^{-1}	813 kg m^{-2} s^{-1}
mean liquid temperature	30.3°C	37.4°C
Reynolds number	30 100	33 500
inner wall heat flux	16 000 W m^{-2}	16 000 W m^{-2}
m.p. pressure	277 kPa	277 kPa.

The mixed-mean liquid velocity at the measurement plane was about 1% higher for the LDV experiment. The mean axial velocity distributions, Fig. 2(a), are in good agreement when this is taken into account.

Discrepancy appeared, however, between the two axial intensity distributions in the inner half of the annulus, Fig. 2(b). The agreement was worse for the radial intensity distribution. On the other hand, a somewhat better agreement was found for the axial Reynolds shear stress distribution.

Scrutiny of these and additional heated flow data at other mass velocities and inner wall heat fluxes led to our view that the CTA turbulence data were affected by the probe as well as by inadequate compensation for liquid temperature fluctuations. Possible reasons for the latter are: (i) relatively large spacing between the CTA velocity and temperature sensors, and (ii) inadequate frequency response of the temperature sensor in R-113, a low thermal conductivity liquid.

To determine the extent of statistical bias in the velocity data, some of the isothermal and heated flow experiments were repeated in the retro-reflect light collection mode. Since the data rate was usually much higher in the retro-reflect mode, it was possible to operate the signal processor as a controlled processor yielding even-time-sampled data. As there should be no bias in even-time-sampled data, a comparison of the results from these data with those from the backscatter mode data would indicate the extent of statistical bias in the latter. Table 1 shows such a comparison for the following experiment:

mass velocity	565 kg m^{-2} s^{-1}
inlet mean liquid temperature	50.2°C
inlet Reynolds number	24 540
inner wall heat flux	16 000 W m^{-2}
m.p. pressure	277 kPa.

The backscatter (bs) and the even-time-sampled retro-reflect (rr) results agree to within 2% for most of the data. On the basis of this and other experiments, statistical bias was judged not to be a significant problem over most of the annulus. It was not possible to carry out this comparison very near the inner wall because the data rate in the retro-reflect mode was not high enough to permit even-time sampling.

To determine whether the cumulative effect, along the beam paths, of the random fluctuations in the liquid refractive index was significant, the backscatter measurements for several heated flow experiments were compared with the corresponding retro-reflect (uneven-time-sampled) measurements. It should be noted that the lengths of the beam paths in the annulus liquid for the retro-reflect measurements were about twice those for the corresponding backscatter measurements. Agreement was quite good for the time-mean axial velocity, axial and radial turbulent intensity, and the $\overline{uv}$ data. It was therefore inferred that the velocity measurements were not significantly affected by the random fluctuations in the liquid refractive index.

Table 1. Comparison of backscatter and retro-reflect velocity data

R^*	0.095	0.207	0.346
$\overline{U}_{bs}$(m s^{-1})	0.3651	0.4035	0.4300
$\overline{U}_{rr}$(m s^{-1})	0.3645	0.4016	0.4199
u'_{bs}(m s^{-1})	0.0333	0.0229	0.0183
u'_{rr}(m s^{-1})	0.0329	0.0231	0.0180
v'_{bs}(m s^{-1})	0.0181	0.0153	0.0139
v'_{rr}(m s^{-1})	0.0174	0.0153	0.0140

RESULTS AND DISCUSSION

Table 2 contains the ranges of variables over which we performed measurements and the associated measurement uncertainties. Much of the velocity field data are presented in this paper in dimensional form because certain important quantitative trends can be identified in this form without ambiguity.

Isothermal flow experiments

Figure 3(a) shows the $\overline{U}$ vs R^* distribution at the m.p. for Reynolds numbers of 18 000, 28 450 and 40 480. The location closest to the annulus inner wall for which data are reported is 0.25 mm ($R^* \approx 0.023$)†. For each Reynolds number, the maximum mean axial velocity occurs at $R^* \approx 0.43$–0.44.

The radial distribution of $\overline{V}$ is not shown for brevity. The measured values were very small compared to the $\overline{U}$ values ($\leqslant 1\%$). This is consistent with the fact that in a hydrodynamically fully developed flow, the mean radial velocity would be zero.

Figure 3(b) contains plots of u' vs R^* for the three Reynolds numbers. At Reynolds numbers of 28 450 and 40 480, u' continues to increase until $y \approx 0.25$ mm. However, at Reynolds number of 18 000, u' peaks farther from the inner wall ($y \approx 0.4$ mm, $R^* \approx 0.037$) and then decreases toward the wall (buffer layer). This is expected, since for the same y^+ value, y is larger for $Re = 18\,000$, the friction velocity at the wall being smaller. The locations of the minima in the u' profiles are very close to the corresponding maximum axial velocity locations. This is also an expected feature.

Figure 3(c) shows the radial distribution of v' for the same three Reynolds numbers. v' is generally smal-

† At $y < 0.25$ mm, the data rate was too low for accurate measurement.

Table 2. Range of experiments and associated measurement uncertainties

	Range	Uncertainity[a]
Reynolds number at test section inlet	18 000, 28 450, 40 480	±100
Wall heat flux	0, 9000, 16 000 W m^{-2}	±100 W m^{-2} (for the nonzero heat fluxes)
Mean liquid temperature at test section inlet	30.3, 31.2°C	±0.1°C
m.p. pressure/R-113 partial pressure at m.p. (sat. temp.)	277 kPa/269 kPa (80.1°C)	±1 kPa (±0.2°C)
Wall (heated) temperature at m.p.	40–54°C	±0.4°C

[a]The uncertainty estimates are for 95% confidence.

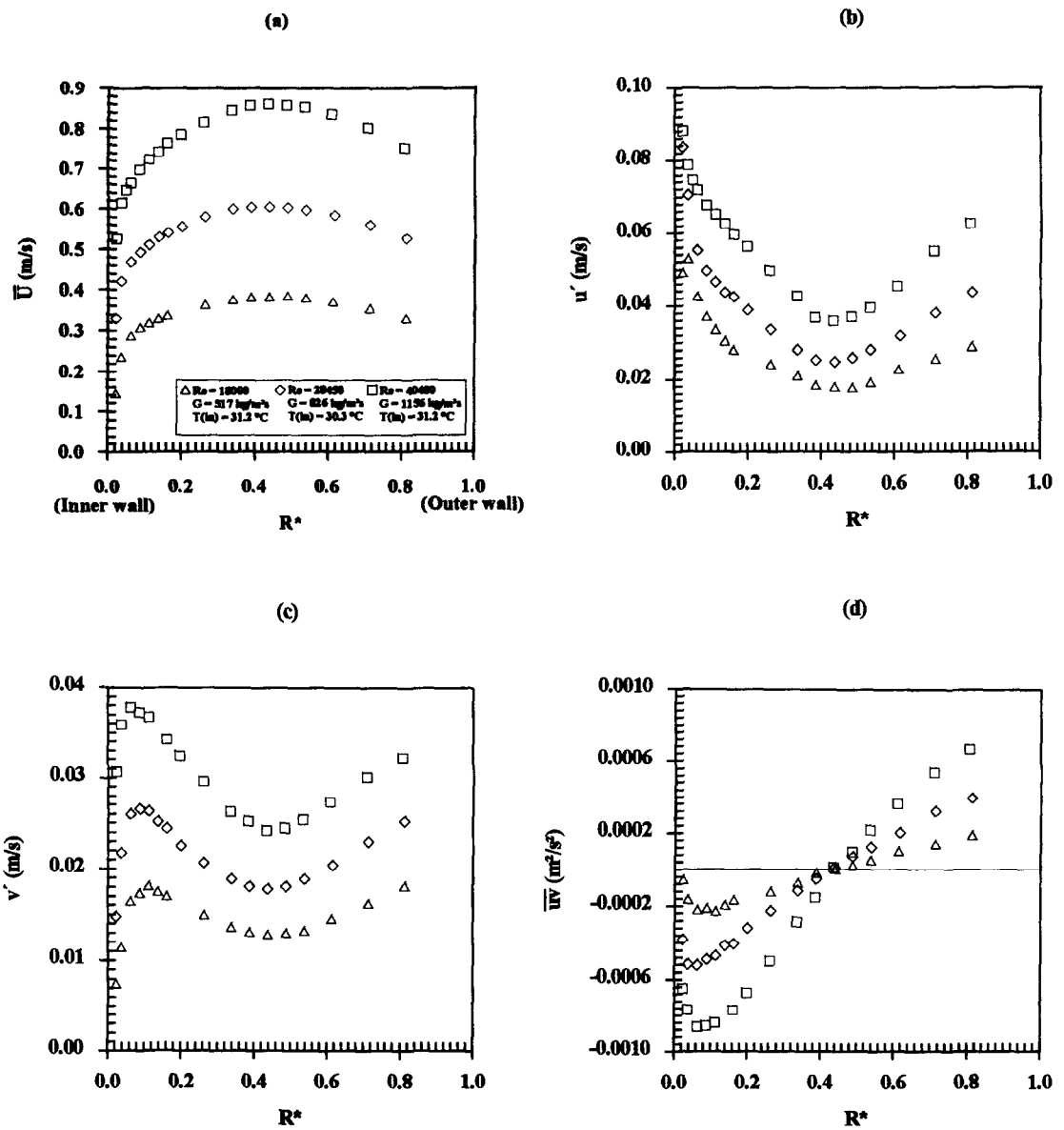

Fig. 3. Measurement in isothermal flow at three Reynolds numbers, (a) mean axial velocity, (b) axial turbulent intensity, (c) radial turbulent intensity, (d) cross-correlation between axial and radial velocity fluctuations.

ler than u'. Also, in comparison with u', v' begins its decrease to the wall value of zero farther from the inner wall at each Reynolds number. The minima in the v' profiles are also near the respective maximum mean axial velocity locations. These are expected characteristics.

Figure 3(d) contains the radial profiles of $\overline{uv}$ for the three Reynolds numbers. The profiles cross the zero value line at $R^* \approx 0.42-0.44$, the locations being very close to, but not necessarily coincident with the maxima of the mean axial velocity profiles. Since the radius ratio, α, of our annulus is 0.417, the flow is only slightly asymmetric, and the deviation of the zero Reynolds shear stress location from that of the maximum mean axial velocity would be small, Rehme [5]. If the radius ratio corresponding to the zero Reynolds shear stress location, β, determined from the data is compared with the value obtained from the empirical relation due to Kays and Leung [19],

$$\frac{\beta-\alpha}{1-\beta} = \alpha^{0.343} \tag{1}$$

the agreement is within 1%.

The friction velocity at the annulus inner wall, u_τ, was estimated from each $\bar{U}$ profile by following Clauser [20]. The mean axial velocity distribution from near the inner wall to $R^* \approx 0.42$ was then plotted in wall coordinates, Fig. 4. In addition to the three isothermal experiments already described, data for three others at comparable Reynolds numbers but at higher liquid temperatures are also shown. The logarithmic relation

$$u^+ = 2.63 \ln y^+ + 5.9 \tag{2}$$

fits the data well for $y^+ > 35$. However, the coefficient of $\ln y^+$ (this being the inverse of von Karman constant) and the additive constant in equation (2) are subject to uncertainty, ± 0.06 for the former and ± 0.4 for the latter. In other words, several other relations fit the data almost as well.

Heated flow experiments

As mentioned earlier, velocity measurements were made at two inner wall heat fluxes (9000, 16000 W m^{-2}) for each Reynolds number. Prior to these, the liquid mean temperature and temperature fluctuation intensity distributions were measured at each condition. In Fig. 5(a–c), the temperature distributions are shown for $Re = 28450$. Near the inner wall, both the liquid mean temperature and fluctuation intensity increase sharply. These lead cor-

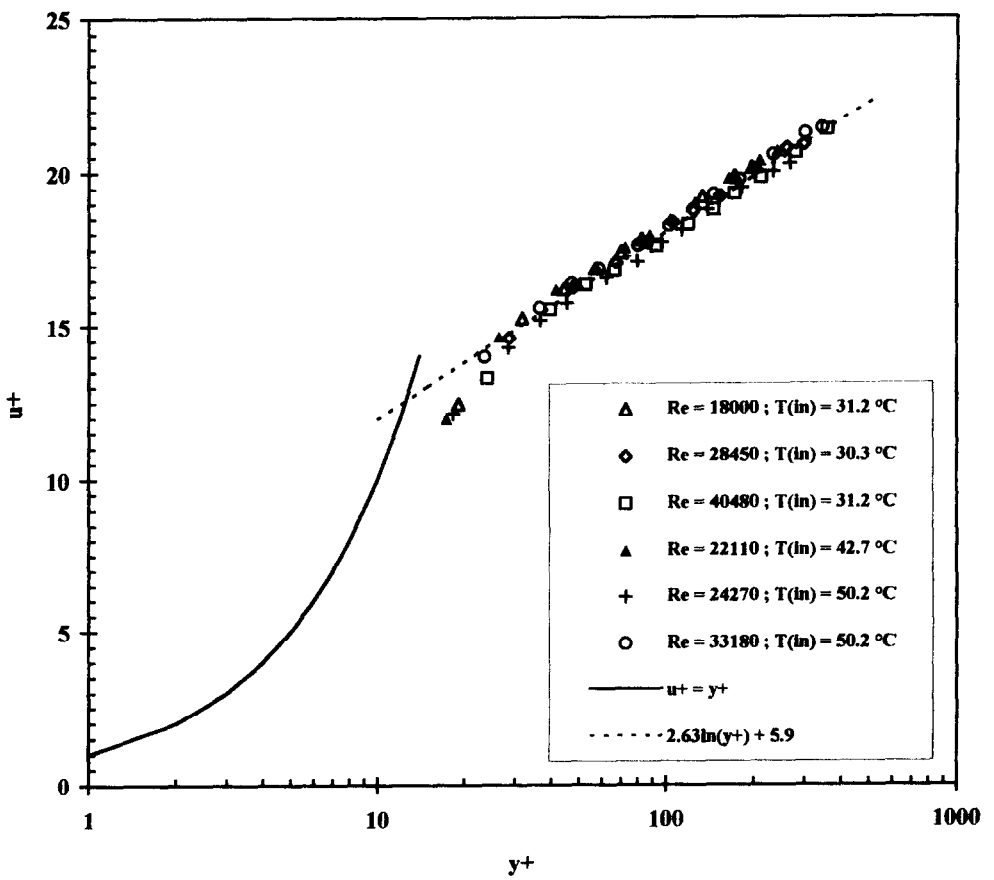

Fig. 4. Mean axial velocity profile in wall coordinates.

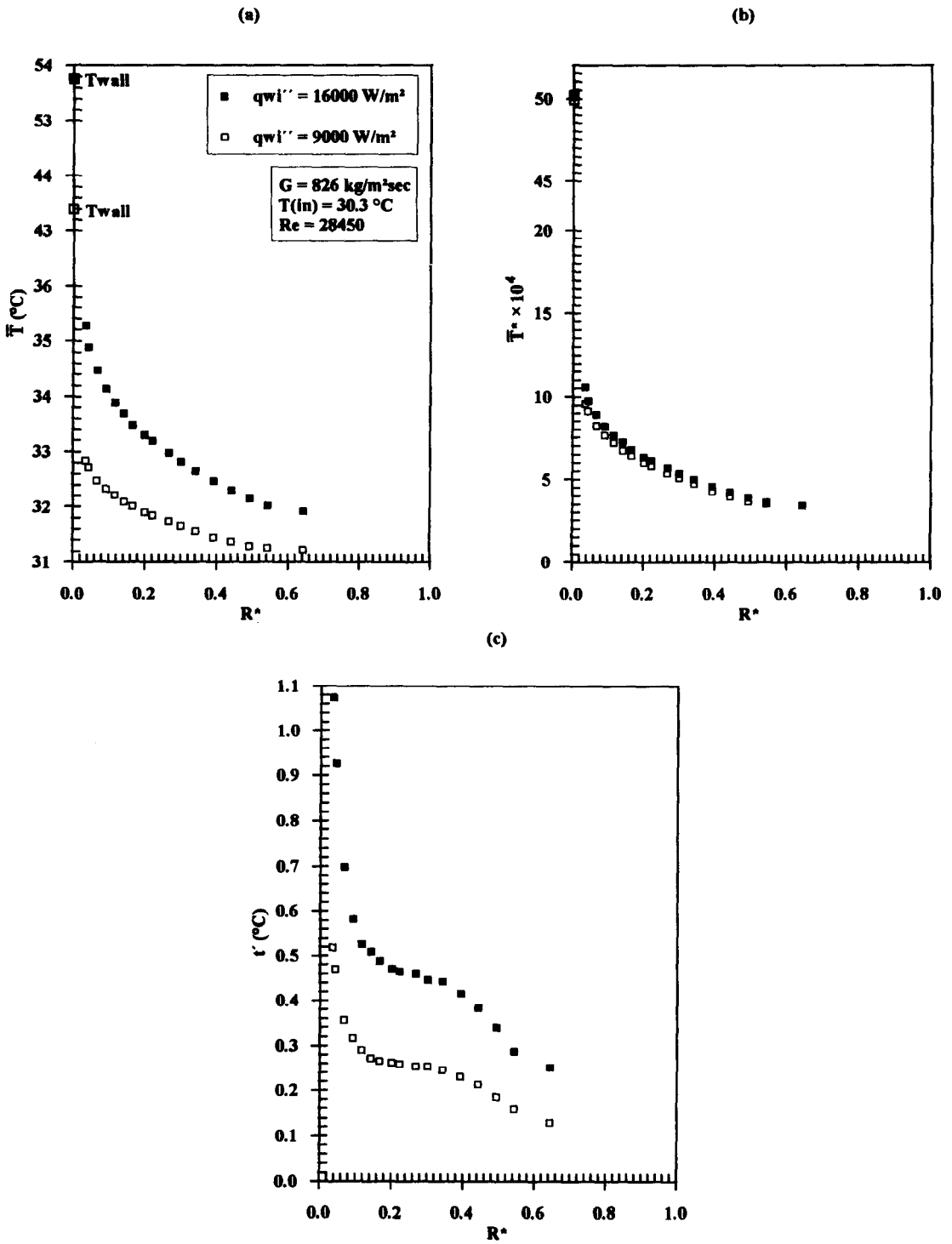

Fig. 5. Temperature field at Reynolds number of 28 450, (a) mean temperature, (b) nondimensional mean temperature, (c) temperature fluctuation intensity.

respondingly to a sharp reduction in the liquid mean refractive index and higher refractive index fluctuation. The former effect was dealt with by careful tracing and steering of the incident laser beams. The effect, if any, of the latter was investigated by comparing backscatter and retroreflect velocity measurements. A probable consequence of the high liquid refractive index fluctuation very close to the heated wall is the less accurate LDV measurement in this region.

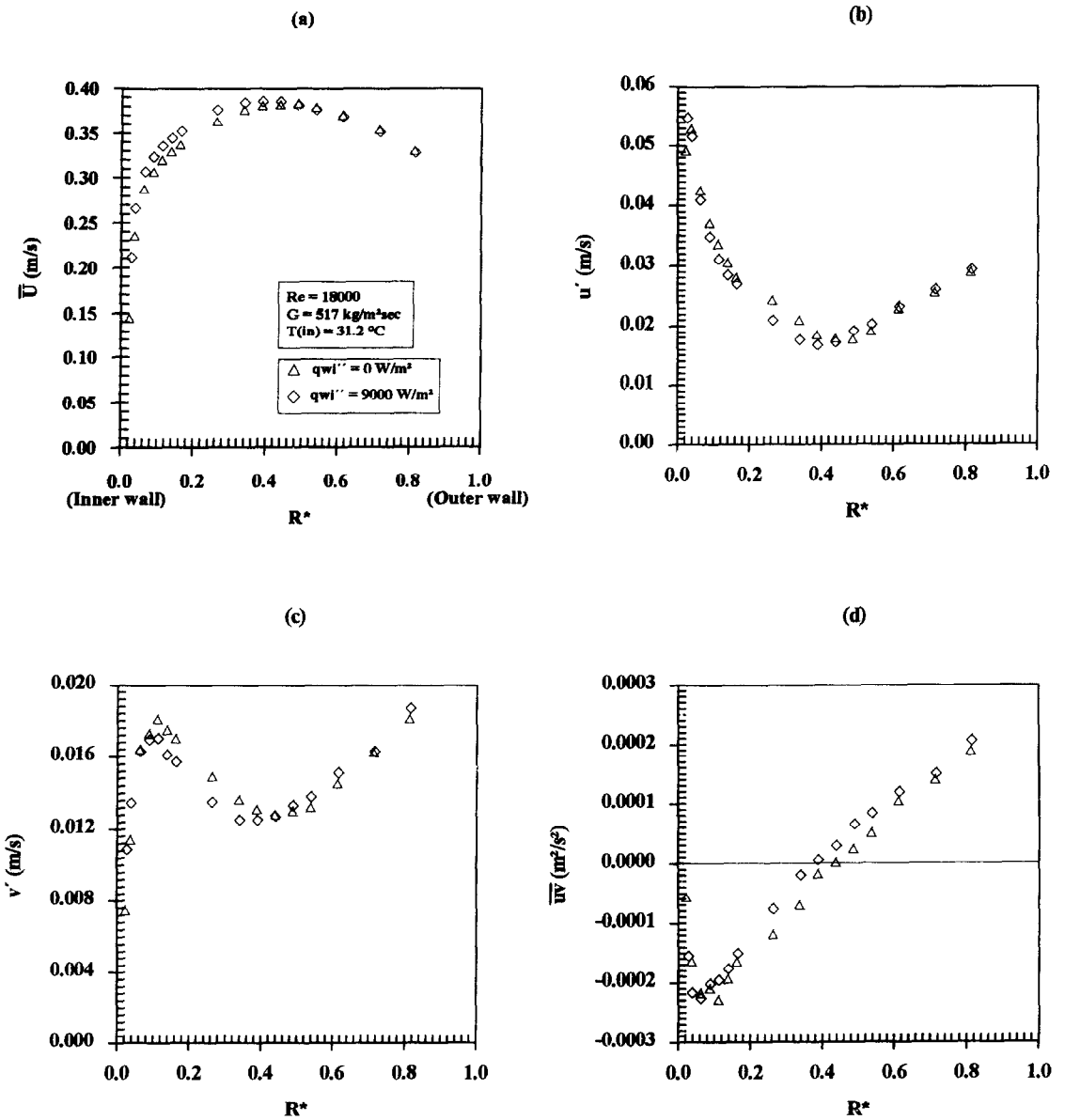

Fig. 6. Measurement in heated flow at Reynolds number of 18 000, (a) mean axial velocity, (b) axial turbulent intensity, (c) radial turbulent intensity, (d) cross-correlation between axial and radial velocity fluctuations.

The velocity field data for heated flow at the three Reynolds numbers are now presented. For clarity of presentation, only the 9000 W m^{-2} data are shown for Reynolds number 18 000 and only the 16 000 W m^{-2} data for Reynolds number 40 480. Data for both heat fluxes are shown for Reynolds number 28 450. In each case, the corresponding isothermal data are shown for comparison.

Figure 6(a–d) contains the radial profiles of, respectively, mean axial velocity, axial turbulent intensity, radial turbulent intensity, and $\overline{uv}$ at Reynolds number of 18 000 and inner wall heat fluxes of 9000 W m^{-2} and zero.

Defining the Grashof number as

$$\frac{g\beta_f(\overline{T}_{wi}-\overline{T}_{bulk})D_h^3}{\nu_f^2},$$

its value for the 9000 W m^{-2} wall heat flux case is approximately 1.9×10^7. The value of Gr/Re^2 is about 0.059.

Figure 6(a) indicates that in the proximity of the heated wall the mean axial velocity remained essentially unchanged from the isothermal value. However, slightly away from the wall ($R^* > 0.05$), the velocity was higher in the heated case, this trend persisting until about the middle of the annulus ($R^* \approx 0.5$). Beyond R^* of 0.5, the distribution gradually approached the isothermal distribution. The

maximum mean axial velocity location shifted perceptibly toward the heated wall, from $R^* \approx 0.44$ in the isothermal case to $R^* \approx 0.41$. The mean radial velocity remained very small ($\leqslant 0.002$ m s^{-1}) across the annulus.

Mass balance based on the measured mean axial velocity and temperature (density) profiles for the heated experiment and the isothermal experiment agreed to within 0.5%.

Figure 6(b) suggests that near the heated wall the axial turbulent intensity remained basically unchanged from the isothermal value.† However, beyond R^* of about 0.07 until $R^* \approx 0.45$, the intensity became lower than in isothermal flow. For $R^* > 0.45$, the intensity first increased to above the isothermal value and then approached the isothermal distribution toward the outer wall. The minimum axial intensity occurred at $R^* \approx 0.40$.

Changes in the radial turbulent intensity profile upon imposition of wall heat flux, Fig. 6(c), were similar to those for the axial intensity except that the increase in radial intensity persisted toward the outer wall (at least to our last measurement location, $R \approx 0.82$). The minimum in the radial intensity profile occurred at $R^* \approx 0.37$.

The radial distribution of $\overline{uv}$ is shown in Fig. 6(d). Close to the heated wall ($R^* \leqslant 0.07$), there was no significant change in $\overline{uv}$ from the isothermal flow. A significant shift of the zero shear stress location toward the heated wall occurred, from $R^* \approx 0.43$ in the isothermal case to $R^* \approx 0.38$. As a consequence, the magnitude of $\overline{uv}$ decreased in the region between $R^* \approx 0.07$ and $R^* \approx 0.38$. The rate of turbulence production would be correspondingly smaller in this region. Examination of the $\overline{uv}$ distribution near the inner wall also suggests a small reduction in the wall shear stress (and hence, in the friction factor) in the heated flow.

Scrutiny of the radial distribution of u'/v' indicates that there was no significant change in the anisotropy of turbulence *vis á vis* these intensities upon imposition of the heat flux.

Figure 7(a–d) contains the radial profiles of, respectively, mean axial velocity, axial and radial turbulent intensities, and $\overline{uv}$ at Reynolds number of 28 450 and wall heat fluxes of 9000 W m^{-2}, 16 000 W m^{-2}, and zero. The mean radial velocity was once again found to be very small ($\leqslant 0.004$ m s^{-1}) across the annulus in all cases and its profiles are not shown.

The Grashof number at 9000 W m^{-2} wall heat flux is about 1.2×10^7 and Gr/Re^2 approximately 0.015. At 16 000 W m^{-2}, Grashof number is about 2.1×10^7 and Gr/Re^2 approximately 0.026.

Alterations in the velocity field in the two heated flows were qualitatively the same as in the case of Reynolds number of 18 000. Quantitatively, there were some differences. At a particular wall heat flux, the increase or reduction in the mean axial velocity, turbulent intensities and $\overline{uv}$ with respect to the isothermal flow were smaller at the higher Reynolds number (28 450). At the same Reynolds number, the alterations were larger at the higher wall heat flux (16 000 W m^{-2}). Furthermore, at the higher Reynolds number, the radial region over which the mean axial velocity increased at a particular wall heat flux did not extend as far from the heated wall as at the lower Reynolds number.

Again, no significant change in anisotropy of turbulence (u' and v') could be discerned. Also, mass balance for the three experiments agreed to within 0.5%.

Figure 8(a–d) shows the radial profiles of, respectively, mean axial velocity, axial and radial intensities, and $\overline{uv}$ at Reynolds numbers of 40 480 and wall heat flux of 16 000 W m^{-2} and zero. The magnitude of mean radial velocity was very small ($\leqslant 0.006$ m s^{-1}) across the annulus in each case.

At wall heat flux of 16 000 W m^{-2}, the Grashof number is about 1.6×10^7 and Gr/Re^2 approximately 0.01.

Alterations in the velocity field in heated flow were, again, qualitatively similar to those at the two lower Reynolds numbers discussed earlier. Quantitatively, the changes for a particular wall heat flux were the smallest at the highest Reynolds number (40 480).

Let us now discuss the effects of buoyancy force on the velocity field. According to Petukhov and Polyakov [12], buoyancy affects the flow field in a heated channel via two mechanisms. Firstly, the buoyancy force acts on the entire flow because of the non-homogeneous fluid density distribution—the so-called *external effect*. This is represented by the *last term* on the right hand side of the axial equation of motion

$$\overline{U}^* \frac{\partial \overline{U}^*}{\partial z^*} + \overline{V}^* \frac{\partial \overline{U}^*}{\partial r^*} = -\left(\frac{\partial P^*}{\partial z^*} - \frac{D_h g_z}{\overline{U}^2_{\text{bulk}}}\right) + \frac{1}{Re} \cdot \frac{1}{r^*} \frac{\partial}{\partial r^*}\left(r^* \frac{\partial \overline{U}^*}{\partial r^*}\right) + \frac{1}{Re} \cdot \frac{1}{r^*} \frac{\partial}{\partial r^*}\left(r^* \frac{\varepsilon}{\nu_f} \frac{\partial \overline{U}^*}{\partial r^*}\right) + \frac{Gr}{Re^2} \Theta. \quad (3)$$

The second effect arises from the fluctuating liquid density in the gravity field. Invoking the local-equilibrium flow assumption, the turbulent energy balance may be expressed as

$$\frac{E^{3/2}}{cL^*} \approx -(\overline{u^* v^*}) \frac{\partial \overline{U}}{\partial r^*} + \frac{Gr}{Re^2} (\overline{u^* t^*}). \quad (4)$$

The left hand side of equation (4) represents the dissipation rate (c is a constant). The first term on the right hand side is the turbulent energy production rate, while the second term represents the contribution of the fluctuating buoyancy force. This direct effect of

† The measurement could be made slightly closer to the inner wall in isothermal flow than in heated flow. This was because of reduction in the data rate in the case of heated flow due to thermophoresis of seed particles.

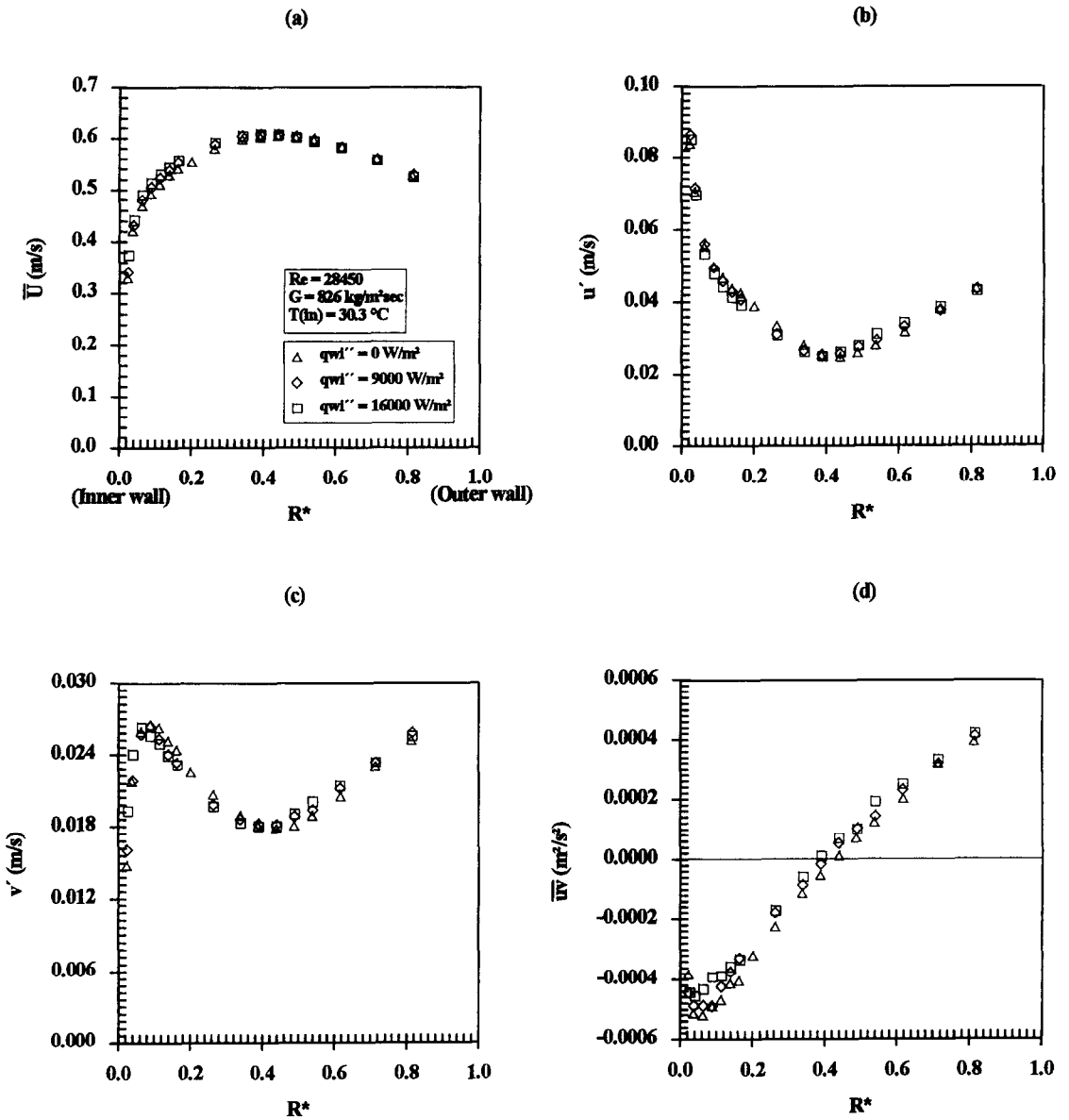

Fig. 7. Measurement in heated flow at Reynolds number 28 450, (a) mean axial velocity, (b) axial turbulent intensity, (c) radial turbulent intensity, (d) cross-correlation between axial and radial velocity fluctuations.

buoyancy on turbulence was termed the *structural effect* by Petukhov and Polyakov, who also stated that the transports of momentum and thermal energy are influenced by a complicated interaction between the structural and external effects of buoyancy.

It should be noted that Gr/Re^2 appears as a factor in both effects. For our flow, the external effect, when significant, would cause the mean axial velocity to increase. As for the structural effect, its influence on the turbulent energy will depend on the sign of the fluctuating buoyancy force contribution in equation (4). Also, changes in the Reynolds shear stress and the mean strain rate will affect turbulent energy production.

In turbulent mixed convection in a vertical channel, the structural effect appears first. Furthermore, the structural effect on the axial velocity appears away from the heated wall first. The external effect would not be significant during this phase of low Gr/Re^2 as in our case. These explain the essentially unchanged mean axial velocity near the heated inner wall and a discernible effect farther from the wall. At higher wall heat fluxes, the external effect is expected to become significant leading to the well-known free convection effect of a fuller mean axial velocity profile near the heated wall.

As for the turbulent kinetic energy, the structural effect does not affect it, at least at low Gr/Re^2, in the proximity of the heated wall. In Fig. 6(b, c), let us consider the region $0.07 \leqslant R^* \leqslant 0.40$, which is farther

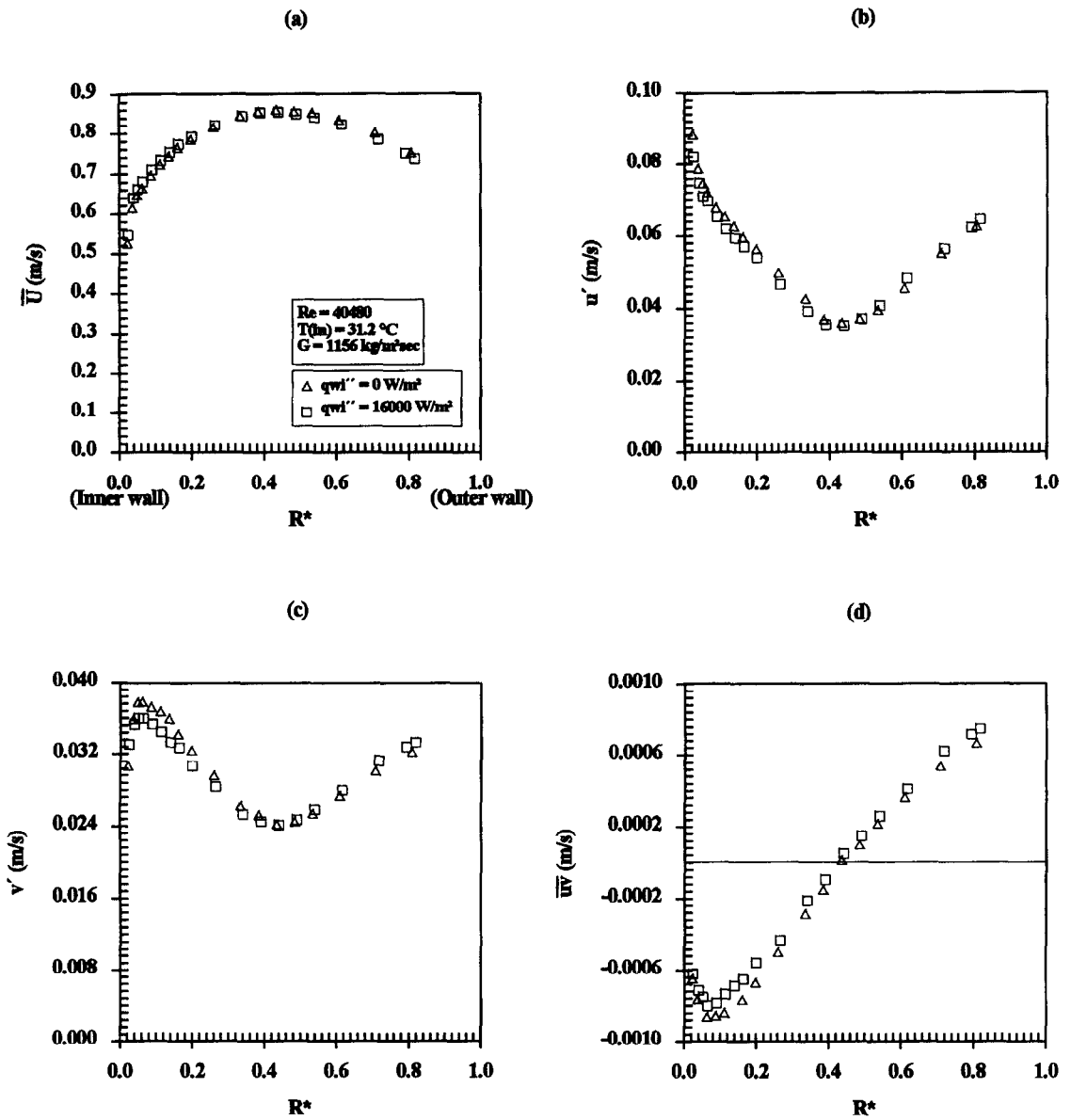

Fig. 8. Measurement in heated flow at Reynolds number of 40 480, (a) mean axial velocity, (b) axial turbulent intensity, (c) radial turbulent intensity, (d) cross-correlation between axial and radial velocity fluctuations.

away from the wall. The fluctuating buoyancy force contribution is expected to be negative here. Also, the production term which is positive decreases in magnitude compared with isothermal flow. Thus, suppression of turbulence would be expected in this region. For $R^* \geqslant 0.41$ (i.e. beyond the maximum axial velocity location), the production term, which is again positive, increases in magnitude†. Figure 6(b, c) shows a discernible increase in the turbulent energy here.

Similar explanations are applicable to the data in Figs. 7(b, c) and 8(b, c).

† At present, we have no information on $\overline{ut}$ in this region.

CONCLUDING REMARKS

In this study, we measured the axial and radial time-mean velocities, turbulent intensities, and single-point cross-correlation between axial and radial velocity fluctuations (~axial Reynolds shear stress) at three Reynolds numbers in upward flow of liquid R-113 through a vertical concentric annular channel. Isothermal flow experiments, as well as experiments in which the annulus inner wall was heated, were performed. In the heated flows, liquid mean temperature and temperature fluctuation intensity distributions were measured. A two-component LDV system was used for the velocity measurements and micro-

thermocouples for the temperature measurements. Laser beam tracing and steering were required in the heated flow experiments.

It was possible to measure velocities quite close to the inner wall ($y^+ \geqslant 18$, depending upon the Reynolds number and wall heat flux). Substantial reduction in the LDV data rate precluded measurement any closer. It was not possible to measure close to the outer wall because of the severity of beam refraction and reflection.

A logarithmic wall law for the inner wall was obtained from the isothermal data. In the heated flows, buoyancy effects were found on the time-mean axial velocity and the turbulence even at very low values of Gr/Re^2. These effects could be explained by utilizing the suggestion of Petukhov and Polyakov that buoyancy affects the turbulent flow velocity field in two ways, one being an effect on the entire flow (the *external effect*) and the other a direct effect on the turbulence (the *structural effect*).

The results presented here should be useful in the development and validation of models for heated turbulent flow of moderate Prandtl number (5–10) fluids. It would be especially interesting to find out whether the observed buoyancy effects can be predicted by the models.

Acknowledgement—This research was supported by the National Science Foundation, Thermal Systems Program, Division of Chemical and Thermal Systems, under grant no. CTS-8918830.

REFERENCES

1. A. Hasan, R. P. Roy and S. P. Kalra, Velocity and temperature fields in turbulent liquid flow through a vertical concentric annular channel, *Int. J. Heat Mass Transfer* **35,** 1455–1467 (1992).
2. J. A. Brighton, and J. B. Jones, Fully developed turbulent flow in annuli, *J. Basic Engng* **86,** 835–844 (1964).
3. A. Quarmby, An experimental study of turbulent flow through concentric annuli, *Int. J. Mech. Sci.* **9,** 205–221 (1967).
4. C. J. Lawn, and C. J. Elliott, Fully developed turbulent flow through concentric annuli, *J. Mech. Engng Sci.* **14,** 195–204 (1972).
5. K. Rehme, Turbulence measurements in smooth concentric annuli with small radius ratios, *J. Fluid Mech.* **72,** 189–206 (1975).
6. R. J. Wilson, Correlation and spectral measurement of fluctuating pressure and velocities in annular turbulent flow, Ph.D. dissertation, Univeristy of Illinois, Urbana-Champaign (1979).
7. M. R. F. Heikal, P. J. Walklate and A. P. Hatton, The effect of free stream turbulence level on the flow and heat transfer in the entrance region of an annulus, *Int. J. Heat Mass Transfer* **20,** 763–771 (1976).
8. N. W. Wilson and J. O. Medwell, An analysis of heat transfer for fully developed turbulent flow in concentric annuli, *ASME J. Heat Transfer* **90C,** 43–50 (1968).
9. K. Hanjalic, Prediction of turbulent flow in annular ducts with differential transport model of turbulence, *Wärme Stoffübertragung* **7,** 72–78 (1974).
10. M. J. Malik and R. H. Pletcher, A study of some turbulence models for flow and heat transfer in ducts of annular cross-section, *ASME J. Heat Transfer* **103,** 146–152 (1981).
11. A. D. Carr, M. A. Conner and H. O. Buhr, Velocity, temperature, and turbulence measurements in air for pipe flow with combined free and forced convection, *ASME J. Heat Transfer* **95,** 445–452 (1973).
12. B. S. Petukhov and A. F. Polyakov, *Heat Transfer in Turbulent Mixed Convection* (Edited by B. E. Launder). Hemisphere, New York (1988).
13. P. K. Jain and R. P. Roy, Stochastic characteristics of vapor fraction and wall pressure fluctuation in boiling flow, *Int. J. Multiphase Flow* **9,** 463–481 (1983).
14. P. Beckman, R. P. Roy, V. Velidandla and M. Capizzani, An improved fast-response microthermocouple, *Rev. Sci. Instrum.* **66,** 4731–4733 (1995).
15. V. Velidandla, S. Putta and R. P. Roy, LDV measurement of turbulent liquid velocity field in channels with curved walls, *Int. Commun. Heat Mass Transfer* **21,** 765–773 (1994).
16. P. Buchhave, W. K. George and J. L. Lumley, The measurement of turbulence with laser-Doppler anemometer, *A. Rev. Fluid Mech.* **11,** 443–503 (1979).
17. R. V. Edwards, Ed., Report of the special panel on statistical particle bias problems in laser anemometry, *ASME J. of Fluids Engng* **109,** 89–93 (1987).
18. L. Talbot, R. K. Cheng, R. W. Scheffer and D. R. Willis, Themophoresis of particles in a heated boundary layer, *J. Fluid Mech.* **101,** 737–758 (1980).
19. W. M. Kays and E. Y. Leung, Heat transfer in annular passages—hydrodynamically developed turbulent flow with arbitrarily prescribed heat flux, *Int. J. Heat Mass Transfer* **6,** 537–557 (1963).
20. F. H. Clauser, The turbulent boundary layer, *Adv. Appl. Mech.* **IV,** 1–51 (1956).